

A Comparative Numerical Study on GEM, MHSP and MSGC

Purba Bhattacharya*, Supratik Mukhopadhyay, Nayana Majumdar and Sudeb Bhattacharya
*Applied Nuclear Physics Division, Saha Institute of Nuclear Physics,
1/AF, Bidhannagar, Kolkata-700064, India*

Abstract

In this work we have concentrated on the detailed understanding of the physical processes occurring in those variants of Micro Pattern Gas Detectors that share micro hole and micro strip geometry. Here, we will present numerical results obtained using the simulation framework, recently developed especially for MPGDs that combines packages such as GARFIELD, neBEM, MAGBOLTZ and HEED. Using this framework, we have estimated quantitatively and qualitatively, some of the important and fundamental characteristics of these MPGDs such as detector gain, transparency, efficiency and their operational dependence on different detector parameters. The estimates have been compared with available experimental and simulation data and an encouraging agreement has been observed.

Keywords: Micro Pattern Gaseous Detectors, MSGC, GEM, MHSP, Detector Modelling and Simulations, Electric Field, Gain, Efficiency

*Corresponding Author: Purba Bhattacharya
Electronic mail: purba.bhattacharya@saha.ac.in

1 Introduction

After the introduction of the microstrip gas chamber (MSGC) [1], several gas detectors based on microstructure devices produced by photolithography processes have been developed. Due to the advantage they provide in terms of improved spatial, energy and time resolution, rate capability, radiation hardness, ageing properties in comparison to more classical configuration, these micro pattern gas detectors (MPGD) are being successfully used in different experiments involving astroparticle physics, high energy physics, medical physics, rare event detection etc. In many applications, MPGD based Time Projection Chambers (TPC) have been envisaged as high-resolution tracking device. Despite the widespread acceptance of MPGDs, thorough understanding of these devices is far from complete. Numerical simulation [2] is an important tool of exploration that can be used to understand detector physics, to analyze their performance and characteristics and improve design for future detectors. Since the physical processes occurring in an MPGD is complex by nature, various software packages need to be used in tandem to simulate different physical aspects that are strongly influenced by the microstructure.

In this paper, we have made an attempt to model and simulate the performance of micro structure devices with micro hole and micro strip geometry, using the recently developed simulation framework Garfield [3, 4] that combines packages such as neBEM [5–8], Magboltz [9, 10] and Heed [11, 12]. Besides providing a framework, Garfield is a code designed to simulate the gaseous detectors, including ionization chambers. It has an interface with the Heed program for simulation of ionization of gas molecules by particles traversing gas-filled chambers. An interface to the Magboltz program is provided for computation of electron transport properties in nearly arbitrary gas mixtures. The electrostatic configuration of the detector determines the regime in which the detector operates. Multiplication of charged particles, formation of avalanche, drift of charged particles and finally the signal collected or induced on relevant detector components also depend on electric field. As a result precise knowledge of the electric field within a detector is critical to proper understanding of the physical processes occurring within a detector and thus detector characteristics.

Over the last few years, the nearly exact Boundary Element Method (neBEM) field solver, has been demonstrated to be a reasonably good candidate for solving electrostatic problem related to gas detectors. As a novel formulation of BEM, neBEM removes some of the major drawbacks of usual BEM and in this work it has been used as an integrated component of Garfield for the estimation of electric field. The solver uses exact analytical expressions for computing the influence of singularity distributions instead of adopting the conventional and convenient approximation of nodal concentration of the charges. Here, the use of analytical solutions of the potential and the electrical field influenced by a uniform charge distribution over a rectangular or triangular boundary element allows nominally exact estimation of the potential and field within the device. Due to the exact foundation expressions, the solver has been found to be exceptionally accurate in the complete physical domain, including the near field and in general free from mathematical / numerical singularities.

In the following, we will highlight the numerical results obtained using the above software combination on MPGDs with micro hole and micro strips. Since the detailed simulation of gaseous detectors begins with the computation of electrostatic configuration within a given device, three dimensional electric field calculation and their variation for different detector parameters have been performed. A comparative study of electric field using two dimensional and three dimensional models shows the importance of three dimensional model for better analysis of detector characteristics. Then we calculate some of the fundamental detector features and their operational dependence on different detector parameters. These studies allow us to optimize such parameters for better detector performance. Some of the estimations, although of a preliminary nature at present, have been compared quite extensively with experimental and numerical results available in the literature.

Section 2, describes a brief overview of the operational principle of the MPGDs studied here. In section 3 the electrostatic configuration of such micro structure devices has been presented. In section 4 and 5 we present the estimations of detector gain, transparency, efficiency of such devices. Comparison with available numerical results, as well as experiments has been described here. Finally in section 6, we have presented our conclusions.

2 Basic Description and Principle

MSGC is historically the first of the microstructure gas detectors. It consists of a set of thin, parallel metal strips deposited on an insulating support and alternately connected as anodes and cathodes. The rear side of the support plate can also have a field-defining electrode, the back plane. A drift plane is placed above. When appropriate potentials are applied to the electrodes, electrons released in the drift space move towards the strips, start to multiply as they approach the high-field region close to the anodes and generate detectable signals. One of the many limitations of MSGC is the fact that the avalanche multiplication does not exceed much, because of breakdown on the insulator surface. After that a number of different electrode geometries were suggested and tested.

Gas Electron Multiplier (GEM) [13] represents one of the many micro hole type detectors, which is very widely used. It is a composite grid consisting of two metal layers separated by a thin insulator which is etched with regular matrix of holes. Applying a voltage between the two conductive plates, a strong electric field is generated inside the holes. The GEM is placed between two planar electrodes. These define the drift (above) and induction (below) electrodes. Thus, GEM separates the gas volume in three regions: a low field drift region above the GEM where the primary charges are produced, a high field region inside the holes where the electrons are multiplied and a transfer region below the GEM where the avalanche electrons drift to the read out electrodes. But the effective gas gain of a single GEM is not very high. The use of GEM as charge pre-amplifier to another micro-pattern detector, or several GEMs in cascade, permits to sustain much larger gains than single stage detectors before breakdown.

One of the more recent MPGDs is the Micro Hole and Strip Plate (MHSP) detector [14, 15], which merges MSGC and GEM characteristics in a single, double-sided element. As designed, it provides two independent charge amplification stages; the holes, operated as a GEM (first stage) and the Micro Strip anodes (second stage), which also function as charge collection electrodes. As in the case of GEM, the first stage amplification of electrons is done inside the hole (g_h : gain inside hole). Then with a suitable difference of potential applied between the cathode and anode strips, the avalanche electrons emerging from the holes are deflected towards the micro strip anodes, where a second amplification (g_s : gain due to strip voltage) occurs. With this design the voltages between the top grid surface and cathode strips, and between the cathode and anode strips, can be maintained well below their breakdown threshold while achieving total gas gain ($g_t = g_h \times g_s$) higher to those obtained with a single GEM or MSGC.

In the following sections, we try to evaluate numerically the fundamental features of MHSP and compare them with GEM as a charge amplifying system. We initiate our work with simple GEM detector modelling and then proceed to analyze MHSP detector. In the process, we have also simulated the MSGC detector to carry out a comprehensive comparison between these detectors with similar geometrical features.

3 Modelling of detector geometry and estimation of electrostatic configuration

While some of the earlier simulations were carried out assuming 2D geometries, 3D modelling is carried out on routine basis in recent times. In order to compare our results with both earlier and recent estimates, we have carried out both 2D and 3D computations. The nature of electric field for a GEM detector has been presented [16, 17] elsewhere using Maxwell [18] field simulator. As an initial comparison, we have modeled GEM, using Garfield, considering standard geometry used in several experiments: 70 μm metal hole diameter, 50 μm kapton hole diameter with 140 μm pitch. We use neBEM to calculate the electric field for this geometry. Though neBEM is a 3D field solver, we can use it to calculate the 2D nature also. For 2D calculation, we have made the geometry such that the length of any one axis of holes becomes considerably large than the other two so that the effect of this dimension has no effect on the electric field in the central part of the hole. Figure 1 shows the cell structure in 2D and 3D models. In this case, we make the length of the hole in the y-direction six times that of the dimension in the x-direction. As a result, in the 2D case, the holes are essentially slots. Figure 2 represents the calculated electric field in the axial and transverse directions. The field computed by using the 3D model differs significantly from

that of 2D as exemplified in this figure.

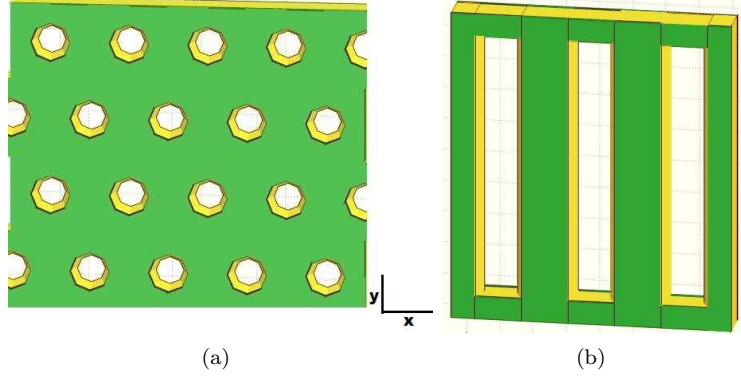


Figure 1: Modeled cell structure of GEM; (a) 3D, (b) 2D

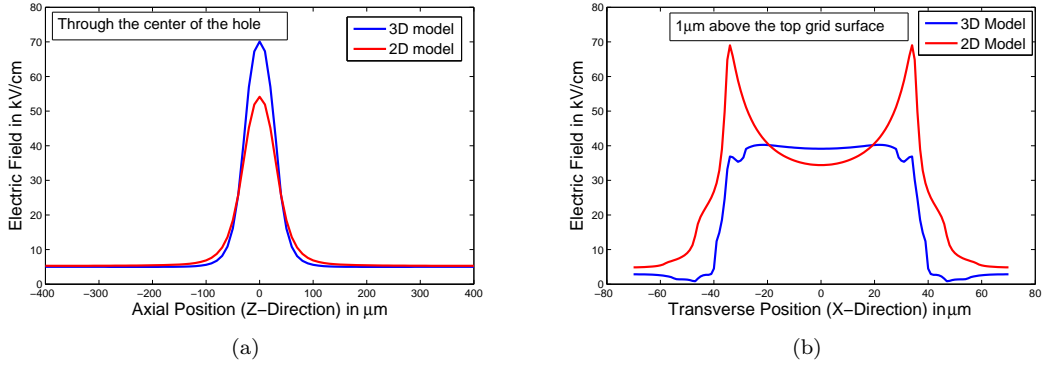


Figure 2: Computed Electric Field of GEM using 2D and 3D model; (a) in the axial direction, (b) in the transverse direction

We have carried out a small numerical experiment to check the effect of hole y-length on electric field in axial and transverse direction while pursuing a 2D calculation. The results shown in Figure 3 illustrate the fact that effect of this y-dimension comes into play when length of the slot is less than 3 times the actual hole diameter. For y-length larger than this value, the assumption to consider the geometry as 2D holds correct.

Following these guidelines, we have modelled MHSP detector, using Garfield considering the dimensions used in reference [19]: 50 μm thick kapton foil with a 5 μm copper coating on both sides. The microstrip pattern on bottom surface of the foil, has a 175 μm pitch with anode and cathode widths of 15 μm and 100 μm , respectively. The anode to cathode gap is 30 μm . The bi-conical holes have 50 and 70 μm diameter in the Kapton and in the copper layer, respectively and are arranged in an hexagonal lattice (two edges of 140 μm and four edges of 190 μm). The used cell structure is depicted in Figure 4. The estimated electric field using neBEM are shown in Figure 5. The nature of electric field in axial direction (Figure 5(a)) and in transverse direction on the top grid surface of MHSP (Figure 5(b)) are similar to that of GEM (Figure 2(a) and Figure 2(b)). The transverse electric field on the bottom microstrip surface is shown in Figure 5(c). Figure 6 presents the variation of electric field in axial direction from the center of the hole to the edge of the hole. From this figure, it is seen that as we proceed towards the edge of the hole, the smooth nature of field is distorted by sharp gradient. Thus the electron drift line in the non-central part of the hole is affected.

It is very interesting to note that by biasing the anode and cathode strips to the same voltage ($V_{ac} = 0V$), the axial electric field through the hole for a single GEM detector and MHSP detector for

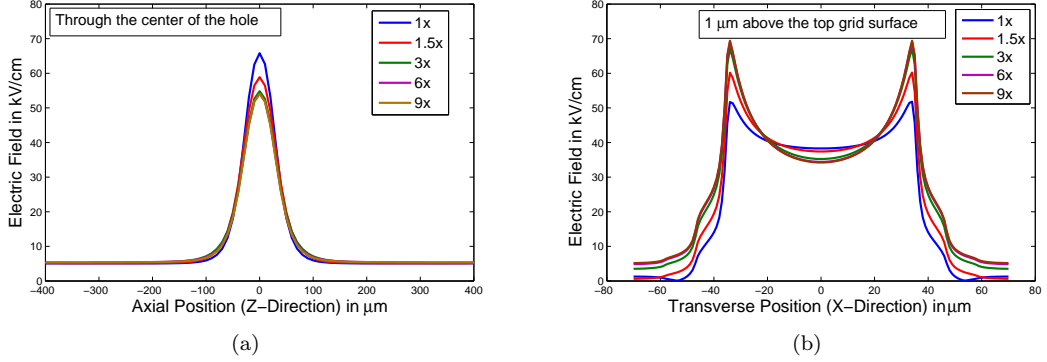


Figure 3: Comparison of electric field for different hole y-length in 2D model (a) in the axial direction, (b) in the transverse direction

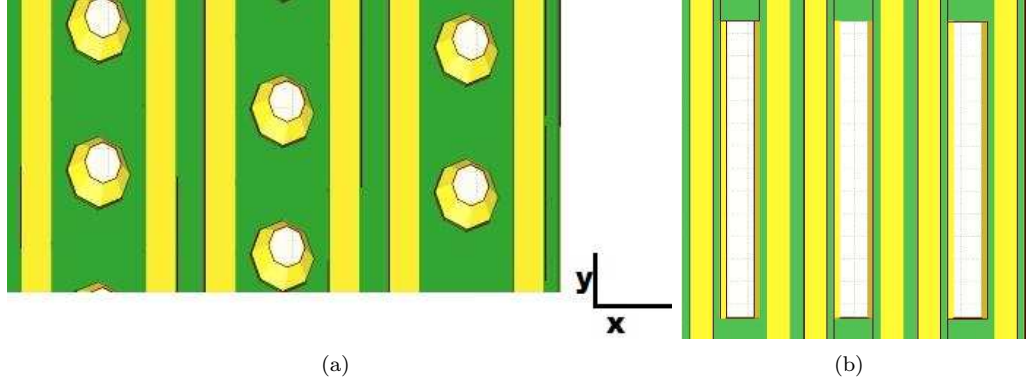


Figure 4: Modeled cell structure of MHSP; (a) 3D, (b) 2D

a fixed hole voltage (V_h) remains the same as shown in Figure 7(a) and thus it is possible to operate the MHSP in a GEM mode. It is also interesting to note that the increase of V_{ac} does not affect the maximum value. So the field inside the hole, does not depend significantly on V_{ac} and it can act as an independent charge amplification stage like GEM. One of the main difference between GEM and MHSP detector is that for GEM, the voltage applied on the bottom induction plane is positive with respect to bottom grid surface, so that on the emergence from the hole, the electrons drift towards the induction plane where they are collected. But in the case of MHSP, the induction plane voltage is negatively biased with respect to the bottom cathode strips voltage, whereas the anode strips are more positively biased than the cathode strips. As a result the electrons are deflected towards the anode strips. The nature of field in the induction region (right hand side) in Figure 7(a) reflects this fact; for GEM, it is about 5 kV/cm, whereas for MHSP, it is about 250 V/cm. The nature of electric field in axial direction in the non-central part of the hole for the above four cases is similar to that of central part, as shown in the Figure 7(b).

Figure 8(a) shows that the field near the top grid surface in the immediate proximity of the hole entrance, is also not influenced by the voltage difference applied to the strips. If we increase the strip voltage from 0V to 220V, the change in the value of electric field is only 5%. A similar observation was also made for Reverse-MHSP [20]. But the change in hole voltage has an direct impact on this field (Figure 8(b)). This means that the electron transport and focussing into the MHSP holes are not affected by V_{ac} and should be studied only as a function of V_h .

Without any hole voltage, the bottom microstrip surface of MHSP, acts as an ordinary MSGC. In Figure 9(a) and Figure 9(b), we have compared the nature of potential and electric field for a MSGC and

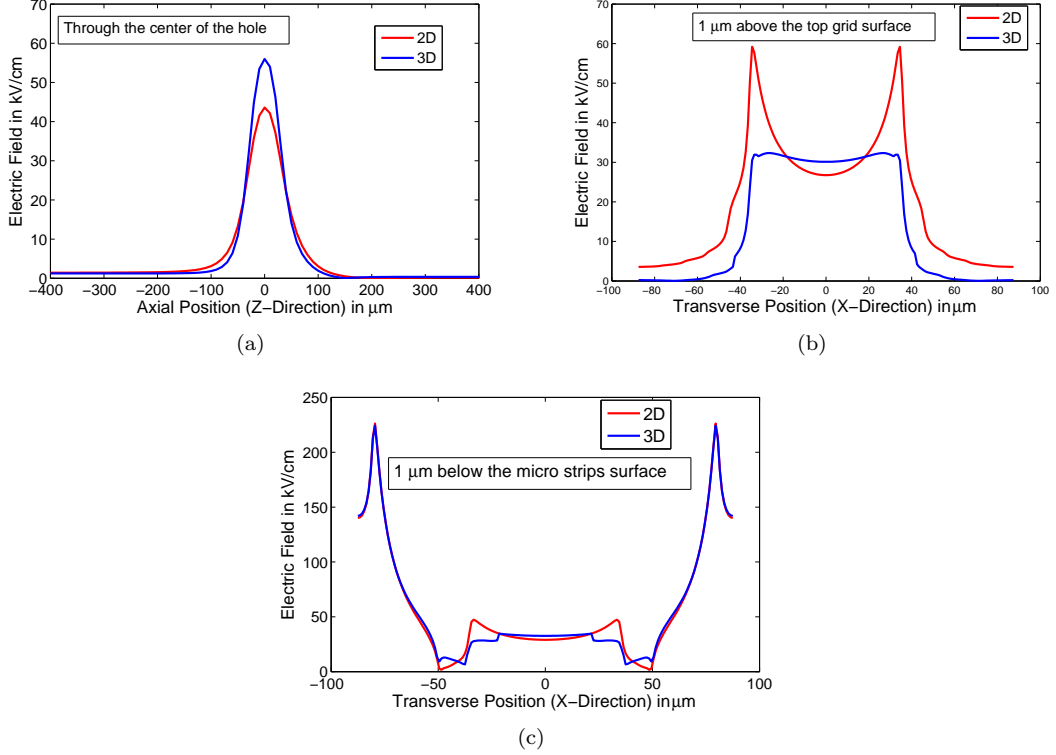


Figure 5: Computed electric field of MHSP (a) in axial direction, and in transverse direction (b) top grid surface, (c) bottom surface

a MHSP without any hole voltage. The nature is similar, the major difference in potential and transverse electric field arising because of the fact that, in MHSP, there is hole between the cathode strips. But the change of hole voltage has an effect on the electric field on the micro strip surface. Figure 9 shows the variation of potential and electric field in the transverse direction for the MHSP in general. A particular V_h is required to drift the electron from the hole to the strips. The change of V_h affects the electric field near the strips. As a result, the gain in second amplification stage (g_s) not only depends on V_{ac} , but also on V_h . The collection efficiency of anode thus depends on V_{ac} as well as on V_h .

This variation of electric field with different voltage determines the regime in which a detector operates and thus controls different detector features such as gain, electron transparency, electron collection efficiency etc, which can be measured experimentally. In the next two sections we try to simulate some of these parameters and compare our results with existing experimental ones.

4 Calculation of gain

4.1 Comparison with 2D simulation results

To evaluate fundamental characteristics of MHSP working under different conditions, a simulation attempt was earlier made using a 2D electric field simulator. So to begin with, we have compared our estimations with those from [14] using a slotted hole version of MHSP. For this we use the detector geometry described in [14]. Pure Xenon gas at a temperature of 293K and 1 atmospheric pressure was chosen.

Using the programs described earlier, the drift, diffusion and avalanche of electrons in the detector were simulated. As in [14], we define two tracks; a set of 30 electrons starting at 240 μm above the MHSP grid and 20 starting at a position 1 μm above the MHSP grid. Figure 10 represents the calculated drift

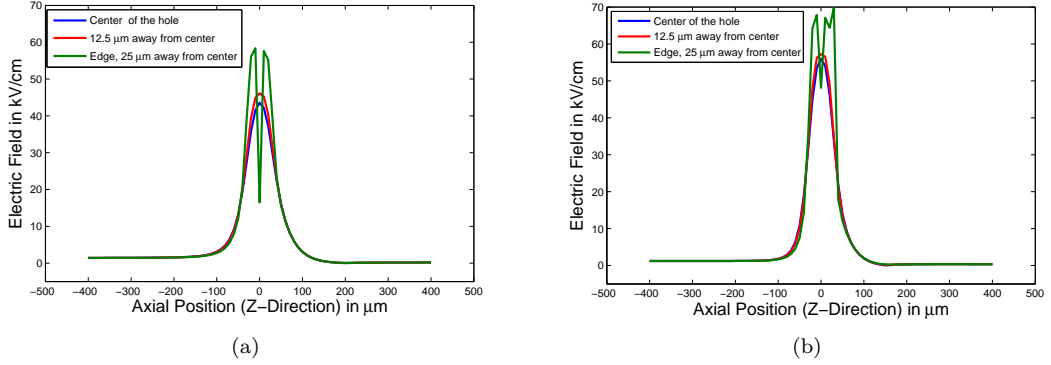


Figure 6: Variation of electric field (in axial direction) of MHSP from the center of the hole to the edge of the hole, (a) using 2D model, (b) using 3D model

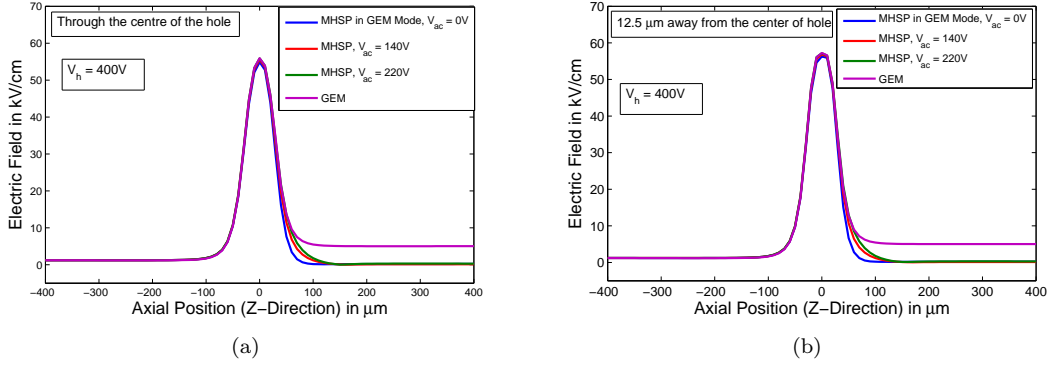


Figure 7: Comparison of axial electric field of GEM and MHSP for a fixed V_h and different V_{ac} through (a) the center of the hole, (b) $12.5 \mu\text{m}$ away from the center of the hole

path of electrons.

In Figure 11(a), we present the calculated results for gain (g_t) as a function of difference of potential between the top grid and the cathode strips (V_h) for fixed V_{ac} of 500V. For a particular V_{ac} , g_t increases with V_h . If we increase V_{ac} , for the same variation of V_h , g_t increases. This nature is reflected in Figure 11(b), where we have shown the variation of g_t with V_{ac} for a fixed V_h .

From these graphs, it is seen that the calculated gain for the electrons starting at the grid plane is higher when compared to the gain obtained for the electrons starting at the drift region. It is expected since in the latter case, electrons started their journey from the lower field region than the electrons in the first case. So the electrons in the latter case, are more focused through the center of the hole due to the high field ratio. In the center, the value of electric field is less than that of non-central part of the hole as shown in Figure 6. After emerging out of the hole to reach the anode, these electrons follow a track which is more distant from the strips than the track of electrons in the first case. The electric field in this distant track has lesser value. As a result, throughout their path, the latter electrons travel under weaker field and so the gain is lower.

Our results follow the trend of variation of gain for two different sets of electrons with different voltages as presented in the work of Veloso et al. [14]. The absolute value of gain, in the present work, is slightly lower than that of previous results. This can be due to the fact that in the earlier work [14] for calculation of gain, a dataset of townsend coefficient from reference [21] was used while we have used the transport table provided by Magboltz in the present case. Since, the mean gas multiplication factor is estimated by exponential integration of this townsend coefficient over the electrons drift path, a small change of value

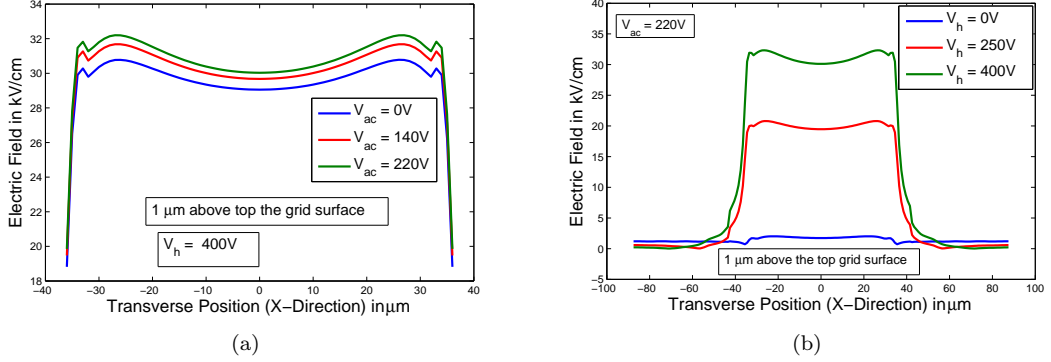


Figure 8: Variation of electric field in the transverse direction in the immediate proximity of hole entrance due to the change of (a) V_{ac} for a fixed V_h , (b) V_h for a fixed V_{ac}

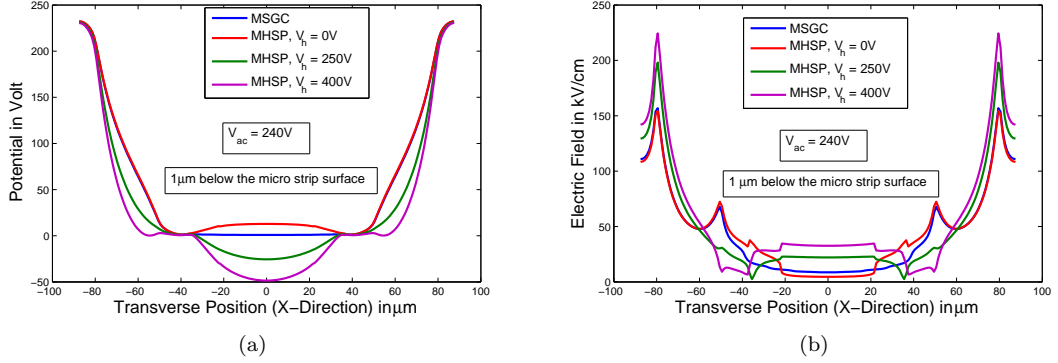


Figure 9: Effect of V_h on the (a) Potential, (b) Electric field in the transverse direction, below the micro strip surface, for a fixed V_{ac}

in this coefficient, can cause a significant variation in the multiplication factor.

4.2 Comparison with experimental results

The above study suggests that electrons arising from different regions of the drift region travel through different tracks to reach the anode strips, resulting in differences in gain. Since in experiment, gamma rays from a radiation source can liberate primary electrons in different part of the drift region, we choose four tracks at different distances above the MHSP top grid surface ($1\mu\text{m}$, $10\mu\text{m}$, $500\mu\text{m}$ and 1mm). The total gain (g_t) is defined as the average gain of the electrons from these four tracks which finally reach the anode strips.

For calculation using 3D model, we use the geometry discussed in section 3. The gas mixture consists of 70% Argon and 30% CO_2 at a temperature of 293K and 1 atmospheric pressure. This mixture is a penning mixture. Different experimental and simulation data [22, 23] have shown that for this mixture about 70% of excited argon molecules that have an energy above the ionisation energy of the admixture will ionise other molecules and thus lead to the increase of gain. Throughout this work we have considered this percentage of transfer rate for this gas mixture.

First we compare our results with one the of the experimental results of GEM detector and also with other simulation data where the estimation of electric field was estimated by Maxwell 3D simulator [23]. Figure 12 shows that the results agree quite well with each other.

Next let us consider the MHSP detector. Figure 13 depicts the total gain (g_t), the gain due to hole (g_h) as a function of V_h maintaining V_{ac} fixed. The gain obtained in the MHSP holes (g_h), when operated

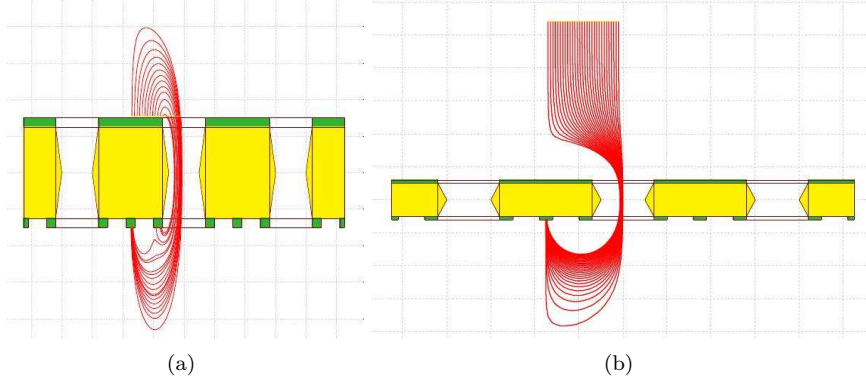


Figure 10: Computed electron drift lines starting their journey from pre-defined track; (a) $1\mu\text{m}$ above the top grid surface, (b) $240\mu\text{m}$ above the top grid surface

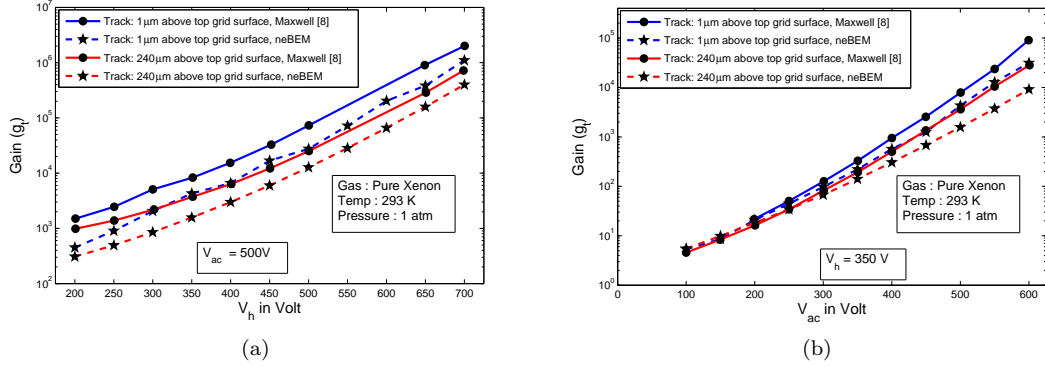


Figure 11: Using 2D model of MHSP, variation of gain with (a) V_h for fixed V_{ac} , (b) V_{ac} for fixed V_h

in GEM mode ($V_{ac} = 0\text{V}$, $g_s = 1$, $g_t = g_h$), is similar to those obtained with single GEM. But for the same variation of V_h , g_t increases with the increase of V_{ac} . Trend obtained from the present simulated estimates is similar to that observed in different experiments [24, 25].

In Figure 14(a), we present the variation in g_t due to variation in V_{ac} for a fixed V_h . Since, g_h for this fixed hole voltage can be calculated from the above procedure (MHSP in GEM mode, $V_{ac} = 0\text{V}$), we can make a rough estimate of g_s , the gain in the 2nd amplification stages. The experimental results [19] verify this nature.

Experimentally it was considered that a fraction of the incident X-rays will interact in the induction region, below the MHSP. The primary electron clouds from these events will only experience one stage of charge multiplication at the micro strip anodes ($g_h = 1$). We make hole voltage 0V and then consider four tracks which are at different distance below the micro strip surface ($1\mu\text{m}$, $10\mu\text{m}$, $500\mu\text{m}$ and 1mm). The electrons from these tracks are collected at anode strips and their multiplication factor depends only on V_{ac} . This value of gain (g_s , when $V_h = 0\text{V}$) is of the same order if we consider a single MSGC, as shown in the Figure 14(b). Then we apply the hole voltage such that the field inside the hole is lower, 6kV/cm which is adequate for only electron transmission but not for electron multiplication. Thus the amplification of electrons from the tracks above the top grid surface of MHSP and below the micro strip surface of MHSP depend only on V_{ac} . The multiplication factor (g_s) of the above four graphs in Figure 14(b) is of the same order. At this value, the hole voltage has no effect on g_s . But this value is lower than the value of g_s given in Figure 14(a). We increase the hole voltage to 400V and then multiplication factor of electrons from the tracks below the micro strip surface agrees with the plot of g_s in Figure 14(a). Thus the hole voltage beyond a certain value has an effect on the electric field on the micro strip surface

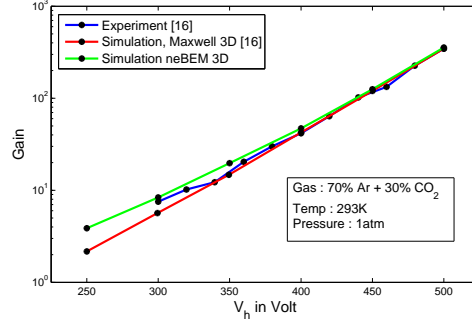


Figure 12: Variation of gain with V_h for GEM

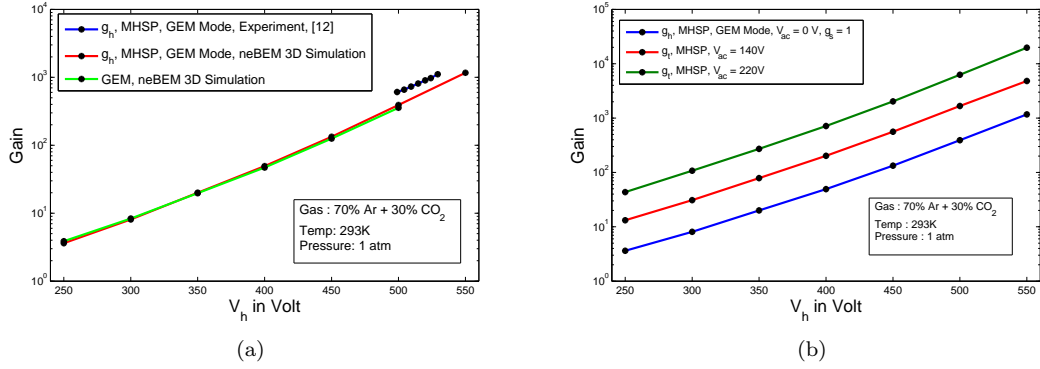


Figure 13: Variation of gain with V_h under different conditions

(Figure 9) which affects g_s .

From the above gain study, it is seen that the total gain of MHSP depends on the potential difference of two different amplification stages. Thus with proper optimization of these two sets of voltages (hole voltage and anode to cathode strip voltage) the total gain of MHSP can be made higher over the single GEM or MSGC, before the breakdown limit.

5 Calculation of electron collection efficiency

Another important parameter, electron collection efficiency of anode (i.e. the fraction of electrons that finally reach the anode strip) was estimated and the variation of this parameter with different voltage settings is discussed in this section.

5.1 Calculation using 2D model

At first, we initiate this work by comparing our estimations with the results presented in [14] using 2D model. Here also, we define two tracks from where the electrons start their journey; $1 \mu\text{m}$ and $240 \mu\text{m}$ above the top grid surface. The variation of electron collection efficiency for the electrons of these two tracks, with different hole voltage and anode to cathode strip voltage is shown in Figure 15(a) and Figure 15(b). Our results agree with previous simulation results.

5.2 Calculation using 3D model

In this section we present estimates of the collection efficiency using a 3D numerical model, discussed in section 3. Figure 16(a) shows the variation with hole voltage for fixed anode to cathode voltage while

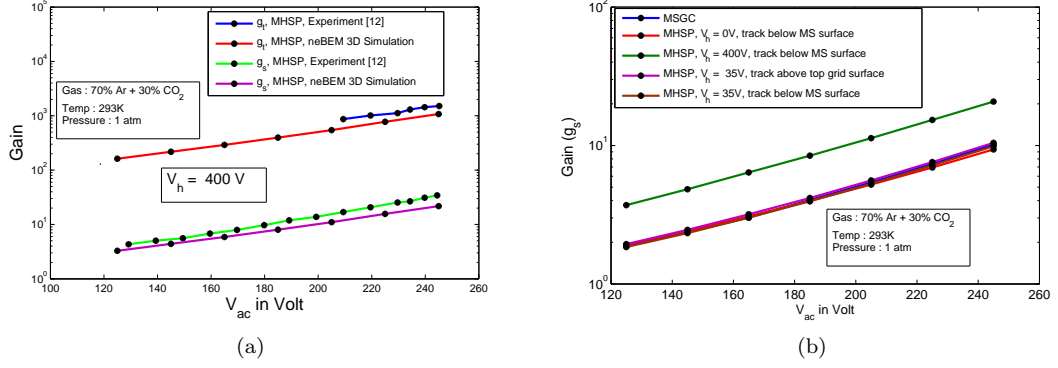


Figure 14: Variation of gain with V_{ac} under different conditions

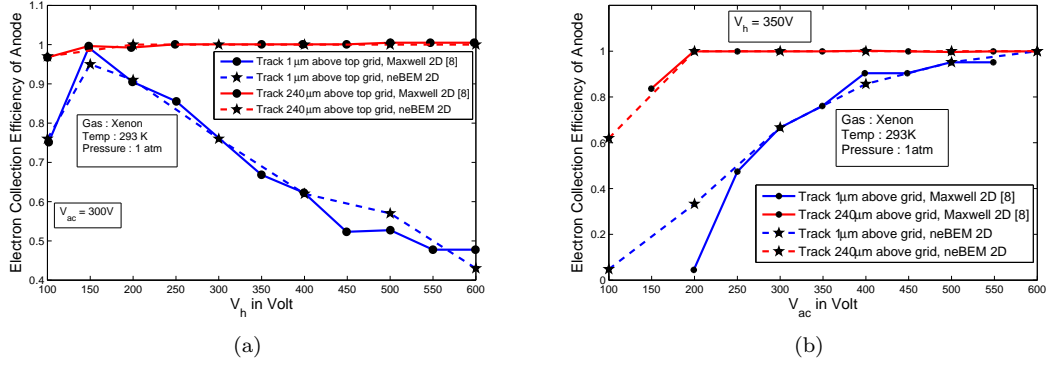


Figure 15: Using 2D model of MHSP, variation of electron collection efficiency of anode, (a) with V_h (b) with V_{ac}

Figure 16(b) presents the variation with anode to cathode voltage for a fixed hole voltage.

An explanation for these results can be made as follows. For a fixed V_{ac} , a minimum V_h is required to focus electrons towards the hole, otherwise the electrons are lost on the top of grid surface. Beyond a certain V_h all the electrons are focused towards the hole and finally collected by anode strips. But if we increase V_h even more, some of the electrons which start their journey close to the grid surface (mainly the electrons whose drift paths are near the edge of the hole) end their journey at the cathode strips (Figure 17(a)) since for them the anode strips voltage is not sufficient to pull them. As a result, the efficiency drops (blue lines in Figure 16(a)). We can increase this efficiency once again by increasing V_{ac} (blue line in Figure 16(b), since for a particular V_h , increase of V_{ac} attracts the electrons more towards the anode strip (Figure 17(b))

Since the electrons which start their journey in the middle of the drift region, mainly drift through the central part of the hole, most of the electrons reach the anode strips safely (red lines of Figure 16(a) and Figure 16(b)). Too much of hole voltage should affect the efficiency as well.

From the above graphs, it is seen that with proper optimization of these two sets of voltage (V_h and V_{ac}), the electron collection efficiency of anode can be kept to a maximum value which ultimately enters into the gain calibration and detector resolution. For this particular geometry, V_h of 500V is suitable (collection efficiency 80%) for two sets of V_{ac} , studied here. At this value of V_h , an increase of V_{ac} certainly improves the efficiency. But this choice of voltage is likely to depend on the sparking rate.

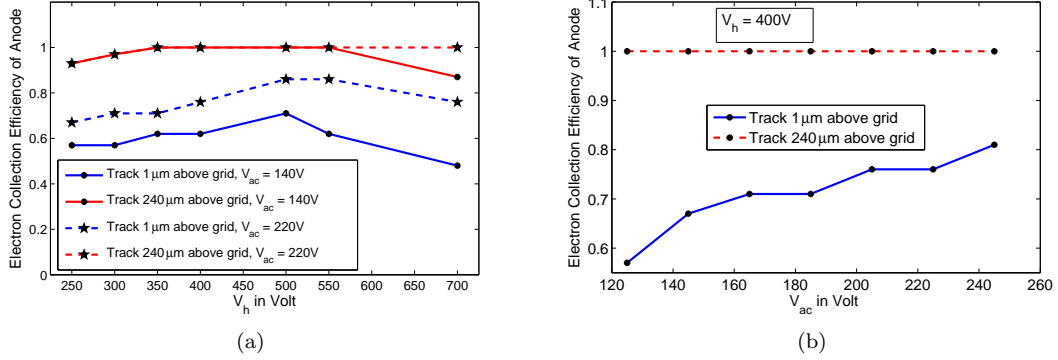


Figure 16: Using 3D model of MHSP, variation of electron collection efficiency of anode, (a) with V_h (b) with V_{ac}

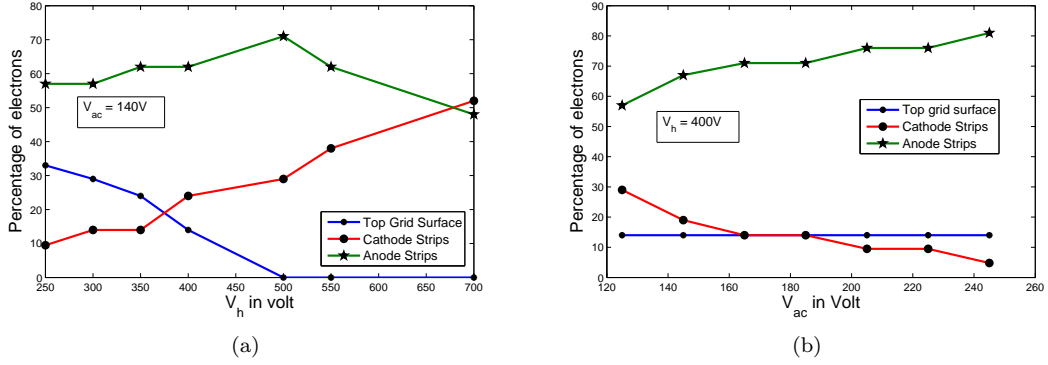


Figure 17: Dependence of electron collection efficiency on different electrode, with (a) V_h for a fixed V_{ac} , (b) V_{ac} for a fixed V_h

6 Conclusion

We have used Garfield+neBEM+Magboltz+Heed combination to simulate the performance of Micro Hole and Strip Plate detector with realistic dimensions. A fairly detailed study of the variation of the 3D electric field, detector gain, collection efficiency depending on several parameters has been carried out. The overall trend as observed in such studies has been found to be in agreement with the existing experimental and simulation results. A comparative study of electric field using 2D and 3D models indicates the necessity of carrying out 3D calculation. The gain study of MHSP detector shows its advantage over single GEM or MSGC and how its functional parameters can be tuned to achieve better device gain and collection efficiency. The well regarded but simplistic Runge Kutta Fehlberg method has provided quite promising results in the present studies. However, microscopic tracking, incorporating the effects of diffusion, attachments etc. will surely lead to more realistic results [26]. While carrying out the computations on one hand, we often found the necessity to have more experimental details than are available in the published literature which may help us to simulate the devices more precisely. On the other hand, there are certain details such as manufacturing defects that were not incorporated in the present modelling.

Acknowledgment

This work has partly been performed in the framework of the RD51 Collaboration. We happily acknowledge the help and suggestions of the members of the RD51 Collaboration.

References

- [1] A. Oed, *Position sensitive detector with microstrip anode for electron multiplication with gases*, *Nucl. Instrum. Methods*, vol. A 263, pp. 351-359, 1988.
- [2] R. Veenhof, *Numerical methods in the simulation of gas-based detectors*, *Jour. Instrum.*, vol. 4, pp. P12017, 2009.
- [3] R. Veenhof, *Garfield - Simulation of gaseous detectors*, online at <http://garfield.web.cern.ch/garfield>.
- [4] R. Veenhof, *Garfield, recent developments*, *Nucl. Instrum. Methods*, vol. A 419, pp. 726-730, 1998.
- [5] S. Mukhopadhyay and N. Majumdar, *A nearly exact Boundary Element Method*, online at <http://nebem.web.cern.ch/neBEM>.
- [6] N. Majumdar and S. Mukhopadhyay, *Simulation of three dimensional electrostatic field configuration in wire chambers: A novel approach*, *Nucl. Instrum. Methods*, vol. A 566, pp. 489-494, 2006.
- [7] S. Mukhopadhyay and N. Majumdar, *Computation of 3D MEMS electrostatics using a nearly exact BEM solver*, *Eng. Anal. Boundary Elem.*, vol. 30, pp. 687-696, 2006.
- [8] S. Mukhopadhyay and N. Majumdar, *A study of three dimensional edge and corner problems using the neBEM solver*, *Eng. Anal. Boundary Elem.*, vol. 33, pp. 105-119, 2009.
- [9] S. Biagi, *Magboltz - Transport of electrons in gas mixture*, online at <http://magboltz.web.cern.ch/magboltz>.
- [10] S.F. Biagi, *Monte Carlo Simulation of electron drift and diffusion in counting gases under the influence of electric and magnetic field*, *Nucl. Instrum. Methods*, vol. A 421, pp. 234-240, 1999.
- [11] I. Smirnov, *Interactions of particles with gases*, online at <http://consult.cern.ch/writeup/heed>.
- [12] I.B. Smirnov, *Modelling of ionization produced by fast charged particles in gases*, *Nucl. Instrum. Methods*, vol. A 554, pp. 474-493, 2005.
- [13] F. Sauli, *GEM: A new concept for electron amplification in gas detectors*, *Nucl. Instrum. Methods*, vol. A 386, pp. 531-534, 1997.
- [14] J.F.C.A. Veloso, J.M.F. dos Santos, C.A.N. Conde, *A proposed new microstructure for gas radiation detectors: The microhole and strip plate*, *Rev. Sci. Instrum.*, vol. 71, pp. 2371-2376, 2000.
- [15] J.F.C.A. Veloso, J.M. Maia, R.E. Morgado, J.M.F. dos Santos, C.A.N. Conde, *The microhole and strip plate gas detector: Initial results*, *Rev. Sci. Instrum.*, vol. 73, pp. 488-490, 2002.
- [16] S. Bachmann, A. Bressan, L. Ropelewski, F. Sauli, A. Sharma, D. Mormann, *Charge amplification and transfer processes in the gas electron multiplier*, *Nucl. Instrum. Methods*, vol. A 438, pp. 376-408, 1999.
- [17] A. Sharma, *3D simulation of charge transfer in a Gas Electron Multiplier (GEM) and comparison to experiment*, *Nucl. Instrum. Methods*, vol. A 454, pp. 267-271, 2000.
- [18] *Maxwell 3D Field Simulator*, online at www.ansys.com.

- [19] J.M. Maia, J.F.C.A. Veloso, J.M.F. dos Santos, A. Breskin, R. Chechik, D. Mormann, *Advances in the Micro-Hole & Strip Plate gaseous detector*, *Nucl. Instrum. Methods*, vol. A 504, pp. 364-368, 2003.
- [20] A.V. Lyashenko, A. Breskin, R. Chechik, J.F.C.A. Veloso, J.M.F. dos Santos and F.D. Amaro, *Advances in ion back-flow reduction in cascaded gaseous electron multipliers incorporating R-MHSP elements*, *Jour. Instrum*, vol. 1, pp. P10004, 2006.
- [21] P.J.B.M. Rachinhas, T.H.V.T. Dias, F.P. Santos, A.D. Stauffer and C.A.N. Conde, *Monte Carlo Simulation of Xenon Filled Cylindrical Proportional Counters*, *IEEE Trans. Nucl. Sci.* vol. 41 984-988 1994
- [22] O. Sahin, I. Tapan, N. Ozmutlu and R. Veenhof, *Penning transfer in argon-based gas mixtures*, *Jour. Instrum*, vol. 5, pp. P05002, 2010.
- [23] S. Dildick, *Avalanche simulations on single GEMs*, *Oral presentation, MPGD meeting 66, 30-08-2011*.
- [24] H. Natal da Luz, J.F.C.A. Veloso, F.D. Amaro, L.F. Requicha Ferreira, J.M.F. dos Santos, A. Breskin and R. Chechik, *MHSP operation in pure xenon*, *Nucl. Instrum. Methods*, vol. A 552, pp. 259-262, 2005.
- [25] J.F.C.A. Veloso, J.M. Maia, L.F. Requicha Ferreira, J.M.F. dos Santos, A. Breskin, R. Chechik and Rui de Oliveira *Recent advances in X-ray detection with micro hole and strip plate detector*, *Nucl. Instrum. Methods*, vol. A 524, pp. 124-129, 2004.
- [26] K. Nikolopoulos, P. Bhattacharya, V. Chernyatin and R. Veenhof, *Electron transparency of a MicroMEGAS mesh*, *Jour. Instrum*, vol. 6, pp. P06011, 2011.